Proceedings of the 2nd Marine Energy Technology Symposium
METS2014
April 15-18, 2014, Seattle, WA

REYNOLDS NUMBER DEPENDENCE OF CROSS-FLOW TURBINE PERFORMANCE AND NEAR-WAKE CHARACTERISTICS

Peter Bachant *
Center for Ocean Renewable Energy
University of New Hampshire
Durham, NH, USA

Martin Wosnik
Center for Ocean Renewable Energy
University of New Hampshire
Durham, NH, USA

ABSTRACT

Minimizing wake losses in wind or marine hydrokinetic (MHK) turbine arrays is a crucial design consideration, as it has a large impact on overall energy production. To understand and mitigate these losses, interactions between turbine wakes must be accurately predicted, with near-wakes being especially important for cross-flow (or vertical-axis) turbines, given their affinity for close-spaced operation. As numerical models become more accurate, validation efforts will need to take into account scale discrepancies between the numerical and physical models and their real-world applications. One such important scaling parameter is the Reynolds number, and it remains unclear what level of confidence can be placed in models validated away from full-scale Reynolds numbers. In other words, what is the minimum acceptable scale mismatch for experimental validation at which models can be said to be "accurate enough?" To address this uncertainty, we investigated—experimentally and numerically—the effects of Reynolds number on the performance and near-wake characteristics of a 3-bladed cross-flow turbine. Mechanical power output and overall streamwise drag were measured in a towing tank at turbine diameter Reynolds numbers $Re_D = U_\infty D/\nu = 0.3\text{–}1.3 \times 10^6$, with performance becoming essentially Reynolds number independent at $Re_D = 0.8 \times 10^6$, corresponding to an average blade chord Reynolds number $Re_c \equiv \lambda U_\infty c/\nu \approx 2.1 \times 10^5$. Detailed measurements of the near-wake one turbine diameter downstream were acquired via acoustic Doppler velocimetry for each Reynolds number case, showing very slight differences in the mean velocity, turbulence intensity, and Reynolds stress at the turbine mid-height plane, i.e., the near-wake statistics were less Reynolds number dependent than the turbine performance. The wake was also simulated using a 2-D Reynolds-averaged Navier–Stokes (RANS) model. The performance results show poor agreement with the experimental data, due to 2-D blockage and the neglecting of blade end effects, however, an increase in performance with Re is predicted. The CFD predictions for wake characteristics are reasonably accurate on the side of the turbine where blades are turning back into the direction of the flow, or where dynamic stall is occurring, but Reynolds number dependence is much more exaggerated compared with the experimental data.

NOMENCLATURE

λ Turbine tip speed ratio $\omega R/U_\infty$.
ν Fluid (water) kinematic viscosity.
ω Turbine shaft angular velocity.
ρ Fluid density.
σ Turbine solidity.
A Turbine frontal area.
c Turbine blade chord length.
C_P Turbine power coefficient.
C_D Turbine rotor drag coefficient.
D Turbine diameter.
H Turbine height.
N Number of turbine blades.
Re_c Approximate turbine blade chord Reynolds number.
Re_D Reynolds number based on turbine diameter.
T Turbine shaft torque.
U_∞ Free stream or tow carriage velocity.

INTRODUCTION

The US Department of Energy predicts a steady growth of contributions from renewable sources to our energy supply, in-

*Corresponding Author: pxL3@unh.edu

cluding from wind energy and marine hydrokinetic (MHK) energy [1]. Toward this end, cross-flow turbines are receiving renewed interest, both for MHK applications in tidal [2], riverine [3] or canal currents [4], as well as for deep-water offshore floating wind farms in the US [5] and Europe [6].

Cross-flow turbines, which can be installed in vertical-axis or horizontal-axis orientation, have some key advantages over axial-flow, horizontal-axis turbines. They are insensitive to variations in flow direction, eliminating the need for a yaw control. They also generally do not require a blade pitching mechanism. For vertical-axis wind turbines, generators and gearboxes can be placed lower in the assembly, increasing stability. This makes vertical axis turbines an attractive option for deep water wind. Cross-flow turbines have some disadvantages when compared to axial-flow turbines, including somewhat lower energy conversion efficiency and unsteady loading of blades/rotor and power train due to their operating principle.

Also of interest are the potential advantages for turbine arrays constructed from cross-flow turbines due to their unique wake dynamics. Firstly, wakes from devices in close proximity have been shown to interact constructively, improving power output of turbines in excess of their stand-alone performance [7]. Secondly, these turbines have been shown to allow more closely spaced arrays compared with conventional axial-flow devices, potentially resulting in more efficient land or channel use [8].

It should be noted that MHK energy conversion is expected to be environmentally benign, for example the first experiments with MHK cross-flow turbines and live fish at two laboratories demonstrated fish survival rates approaching 100%, close to indistinguishable from control populations [9, 10].

To effectively design individual cross-flow turbines and cross-flow turbine arrays it is important to understand the kinetic energy conversion process and the resulting turbine wake and its recovery, in particular the near-wake structure, to accurately predict interactions between turbine wakes of closely spaced devices.

Generally, analytical and numerical predictions used in engineering are tested with physical models, for which it is often impractical, cost prohibitive, or impossible to match all relevant scales, e.g., the Reynolds number, based on on turbine diameter, Re_D, or blade chord, Re_c. In these cases, it is important to be aware of the effects of these scale discrepancies, since a "validated" model may in fact produce unreliable predictions if extrapolated to full-scale.

As it remains unclear what level of confidence can be placed in models validated away from full-scale Reynolds numbers, in the present study the effects of Reynolds number on the performance and near-wake characteristics of a 3-bladed cross-flow turbine were investigated—both experimentally and numerically. Mechanical power output and overall streamwise drag were measured in a towing tank over a range of turbine diameter Reynolds numbers of $Re_D = 0.3\text{–}1.3 \times 10^6$. Detailed measurements of the near-wake one turbine diameter downstream were acquired via acoustic Doppler velocimetry for each Reynolds number case, from which differences in the mean velocity, turbulence intensity, and Reynolds stress profiles are highlighted. The turbine and its near-wake were also simulated using an unsteady 2-D Reynolds-averaged Navier–Stokes (RANS) model. In this paper the numerical results are compared with the experimental data, evaluating this particular model's ability to predict various quantities of interest and how these change with Reynolds number.

Effects of Reynolds Number

For axial-flow (commonly referred to as horizontal-axis) turbines, small changes in angle of attack α of the local relative wind w.r.t. blade chord occur throughout blade rotation, and are due to mean shear in the boundary layer (which can also cause varying deformation) or turbulence. This means it's relatively easy to predict turbine performance with models that employ static foil section data, e.g., blade element momentum (BEM) methods.

For cross-flow turbines, on the other hand, dramatic oscillations in α occur as a blade rotates about the turbine axis, and turbine blades are often undergoing dynamic stall during peak power output, which exceeds predictions based on static foil data [11]. Even so, static foil performance data, e.g. [12], show a strong dependence of $(C_L/C_D)_{\max}$ on (Re_c), with magnitude of $(C_L/C_D)_{\max}$ and α at which $(C_L/C_D)_{\max}$ occurs increasing with increasing Re_D. It follows that cross-flow turbine performance should also depend on Reynolds number, which is shown in, e.g., [13]. Bravo et al. [14] observed Reynolds number independence in power production for a vertical-axis turbine in a wind tunnel for $Re_D = O(10^6)$, where O indicates order of magnitude, though it is unclear whether relevant wake statistics follow the same trend.

Since utility-scale cross-flow turbines will reach $Re_D = O(10^7)$, in this study we sought to investigate/confirm Reynolds number independence of performance around $Re_D = O(10^6)$, but more importantly the dependence on detailed wake characteristics, since these are the drivers of wake recovery, and therefore array performance.

EXPERIMENTAL SETUP

Turbine Model

A three-bladed vertical-axis rotor was developed by the University of New Hampshire Center for Ocean Renewable Energy (UNH-CORE) [15], in the spirit of, but not geometrically identical to, the DOE Reference Model turbine designed by Sandia National Laboratory in 2011 [16], dubbed "RVAT" (Reference Vertical Axis Turbine) or "RM2" (Reference Model 2). An initial design rendering (not shown in [16]) depicted two vertical axis rotors installed in close proximity.

The UNH-RVAT is a 1 m diameter, 1 m tall three-bladed cross-flow turbine, constructed from 0.14 m chord NACA 0020 blades, resulting in a solidity $s = Nc/(\pi D) = 0.13$, which is somewhat higher that of the Sandia RVAT rotor [16]. For this experiment, the blades were fixed at half-chord and mid-span, with zero preset pitch. The blade attachment struts were also built from NACA 0020 foils, and fixed to a 9.5 cm diameter shaft. A drawing of the UNH-RVAT turbine is shown in Figure 1.

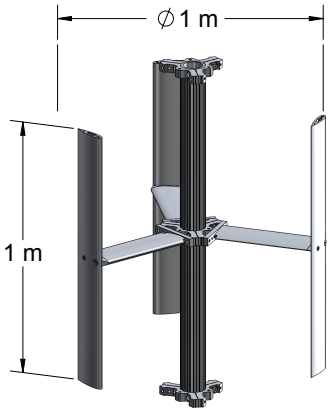

FIGURE 1. CAD DRAWING OF THE UNH-RVAT WITH COUPLING HUBS INSTALLED.

Facility and Instrumentation

Experiments were performed in UNH's tow/wave tank, a 36.6 m long facility with a 3.66 m wide by 2.44 m deep cross-section. Carriage motion is actuated by a permanent magnet servomotor and timing belt, providing highly accurate tow velocities, which are also measured independently by a 10 μm resolution linear encoder.

The turbine was installed in the tow tank's turbine test bed support frame, which is built from NACA 0020 struts, mounted to the carriage via linear bearings, allowing a pair of 2.2 kN capacity S-beam load cells to measure total streamwise drag (also called thrust). The model turbine had an 11% blockage ratio based on its frontal area. The turbine shaft was loaded by a servo motor and gearhead, which provided precise control of mean turbine tip speed ratio. Shaft torque was measured with an Interface T8 200 Nm capacity inline torque transducer mounted between the servo motor and turbine shaft. Signals from the torque transducer and drag load cells were sampled at 2 kHz via National Instruments 9205 and 9237 modules, respectively. Turbine shaft angle was sampled from the servo drive's 10^5 count/rev emulated quadrature encoder output by a National Instruments 9401 counter module. Turbine power was calculated from the measured torque and angular velocity, which was computed by differentiating the shaft angle time series with a second order central difference scheme. Turbine shaft torque was corrected for bearing friction by adding a tare torque, measured in air by driving the turbine shaft with the servo motor. Similarly, drag values were corrected by subtracting the tare drag, measured by towing the test frame with the turbine removed. A schematic of the turbine and instrumentation installed in the tank cross-section is shown in Figure 2 and a photograph of the experimental setup with the RVAT installed is shown in Figure 3.

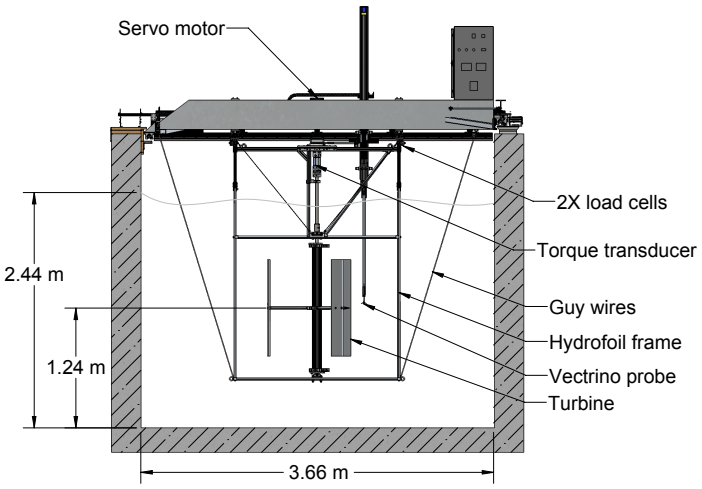

FIGURE 2. SCHEMATIC OF THE EXPERIMENTAL SETUP.

A Nortek Vectrino+ acoustic Doppler velocimeter (ADV), sampling at 200 Hz, was used to measure wake velocity. The device is capable of measuring all three orthogonal components of velocity simultaneously with an accuracy of $\pm 0.5\%$ its measured value ± 1 mm/s. The ADV was mounted on an automated vertical and cross-stream positioning system at 1 turbine diameter downstream $(x/D = 1)$ from the turbine axis, the coordinate system for which is shown in Fig. 4. The turbine was towed through the tank at constant velocity. Tip speed ratio was set via the servo drive and its mean value held constant $(\lambda = 1.9)$ during each tow. To ensure repeatability of experimental conditions, an appropriate minimum tank settling time between tows for each tow speed was determined using ADV measurements taken after a tow at each speed.

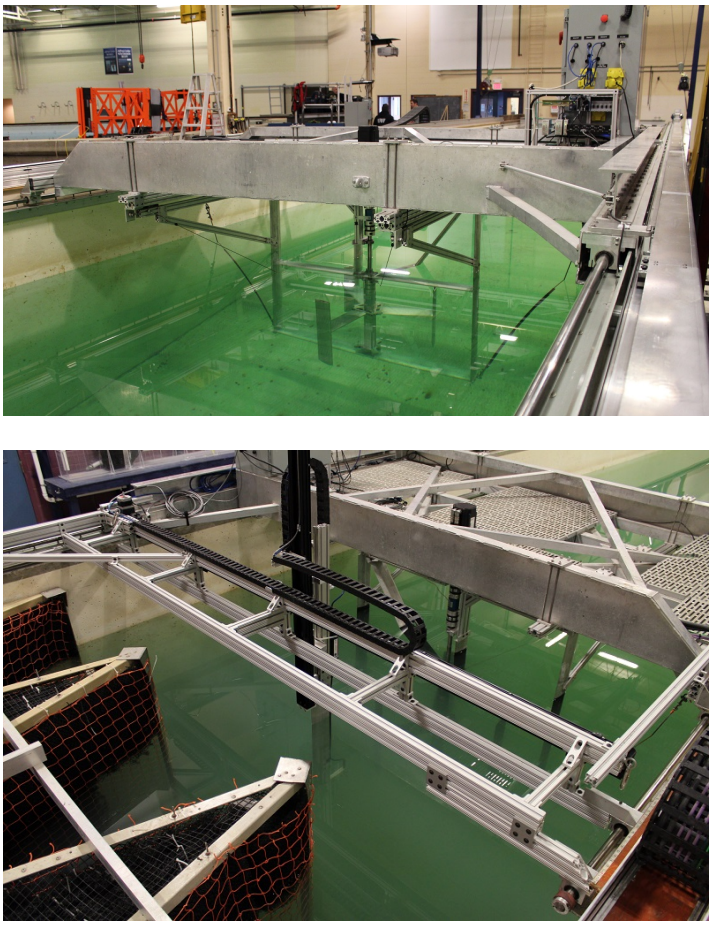

FIGURE 3. PHOTOGRAPHS OF THE EXPERIMENTAL SETUP IN THE UNH TOW/WAVE TANK WITH RVAT INSTALLED.

PREVIOUS CHARACTERIZATION OF THE UNH-RVAT

Baseline experiments with the UNH-RVAT previously reported in [15] included measurements of rotor power, drag (or thrust), tip speed ratio, and detailed maps of mean flow and turbulence components in the near-wake at a single Reynolds number. This baseline performance data are also being used by Sandia National Laboratories to validate their CACTUS performance prediction model for the US Department of Energy Reference Model turbines [18].

Representative turbine power and drag coefficients are shown in Figures 5 and 6, respectively. The drag coefficient curve increases monotonically with tip speed ratio, as expected. The power coefficient curve also looks similar in shape to previous experiments with vertical axis turbines, reaching a maximum value of 26% at a tip speed ratio $\lambda = 1.9$. It should be noted that the UNH-RVAT was not designed to have the highest power coefficient possible, only to provide a high fidelity data set for a simple turbine model at reasonably high Reynolds numbers. Also note that the power coefficient for higher-solidity turbines

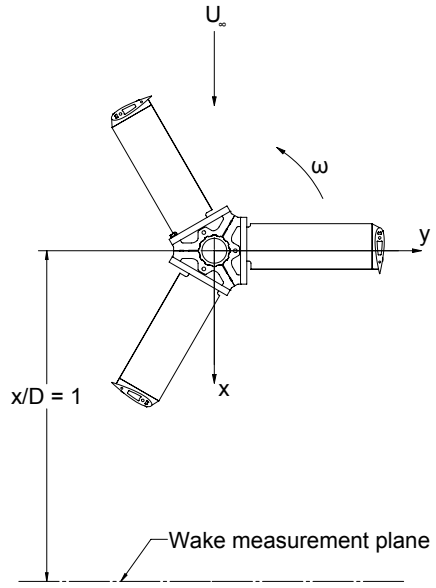

FIGURE 4. TOP VIEW OF TURBINE AND MEASUREMENT COORDINATE SYSTEM.

of this type is quite sensitive to blade mounting location, and can likely be improved, c.f. [17].

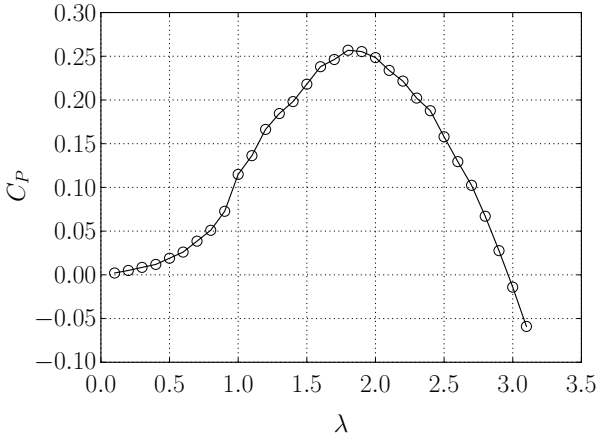

FIGURE 5. MEASURED TURBINE POWER COEFFICIENT VERSUS TIP SPEED RATIO, FROM [15].

In the previous experiment, transverse wake profiles in the near-wake at $x/D = 1$ were obtained at various heights from the horizontal turbine center plane up to $z/H = 5/8$, with a range of $y/R = \pm 3$, as shown in Figure 7. Here $z/H = 0$ corresponds

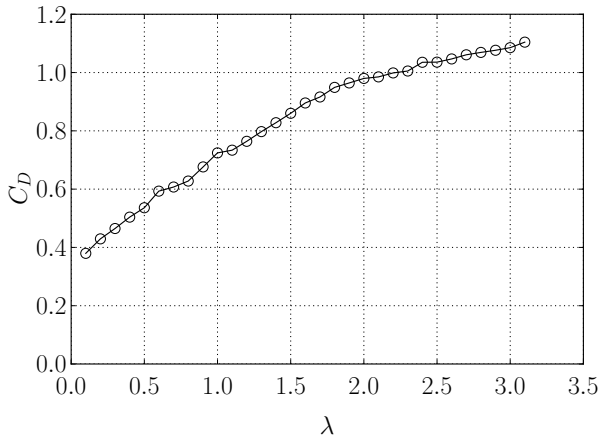

FIGURE 6. MEASURED TURBINE DRAG COEFFICIENT VERSUS TIP SPEED RATIO, FROM [15].

to the half-height (center) of the turbine. Mean and fluctuating streamwise velocity contours for the turbine operating at a tip speed ratio $\lambda = 1.9$, corresponding to maximum power output in Figure 5, are shown in Figure 8. These plots show, in a statistical sense, the complex asymmetry and three-dimensionality of the wake of this turbine. The flow is seen to accelerate around the turbine due to blockage, also creating strong downward mean flow and streamwise vorticity. The peak momentum deficit occurs away from the center line at positive values of y/R, while the majority of turbulence intensity occurs around $y/R = -1$, showing evidence of separated flow, likely due to blades in dynamic stall, and also near the top of the turbine, due to blade tip vortex shedding. Turbulence was found to be approximately locally isotropic at $x/D = 1$, i.e., σ_v and σ_w contours are similar to those of σ_u shown in Figure 8 [15].

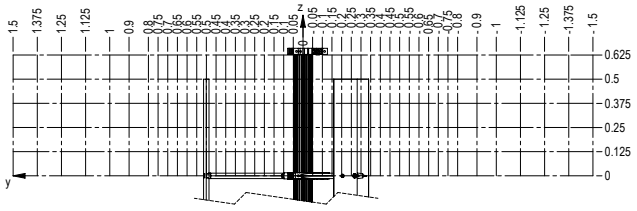

FIGURE 7. FRONT (DOWNSTREAM) VIEW OF TURBINE WAKE MEASUREMENT LOCATIONS FROM [15]. DIMENSIONS ARE IN METERS

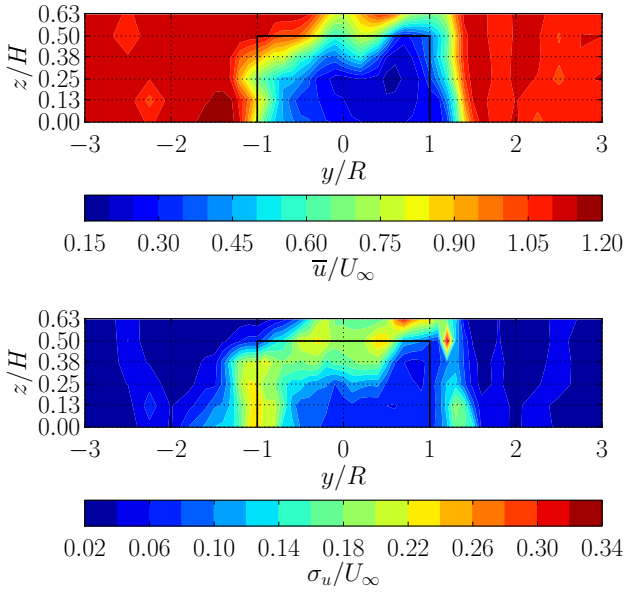

FIGURE 8. CONTOURS OF NORMALIZED STREAMWISE VELOCITY MEAN (TOP) AND STANDARD DEVIATION (BOTTOM) AT $x/D = 1$ AND $\lambda = 1.9$, FROM [15]. SOLID BLACK LINES INDICATE TURBINE FRONTAL AREA.

NUMERICAL SETUP

The numerical model used here is based on an unsteady Reynolds-averaged Navier-Stokes (RANS) approach. The two-equation k–ω SST turbulence model [19] is used to close the equations. The k–ω SST (shear stress transport) formulation combines the desirable features of the standard k–ω model (by Wilcox) to be well-behaved in adverse pressure gradient and separating flows (essential for cross-flow turbines) with the desirable features of a standard k–ε closure model in the free stream. The numerical model was implemented in the open-source CFD platform OpenFOAM version 2.3.0.

The UNH-RVAT geometry is located inside a two dimensional mesh, containing a circular rotating region, which is matched to a larger, non-rotating domain that extends 1.52 m upstream and 2.16 m downstream from the turbine axis. Simulations were tested for sensitivity to mesh refinement, which initially showed poor results (judged by comparison to the experimental data) for very fine mesh resolution, thus a slightly coarser mesh was chosen. Nonetheless, the final mesh is still highly resolved with viscous lengths on the surface of the foils, $y^+ \equiv u_* y/\nu \sim 1$. A sample mesh used for the 2-D simulation is shown in Figure 9. For each Reynolds number case—since viscosity is the only parameter adjusted to change Reynolds number—the entire mesh is scaled proportionally such that y^+ at the first cell next to the turbine blades is approximately equal for all. Boundary conditions at the walls are set to mimick a towing

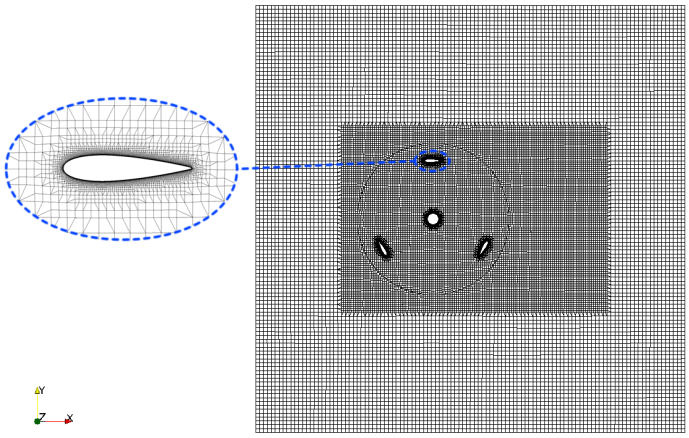

FIGURE 9. SNAPSHOT OF THE TWO-DIMENSIONAL COMPUTATIONAL MESH FOR $Re_D = 1.0 \times 10^6$.

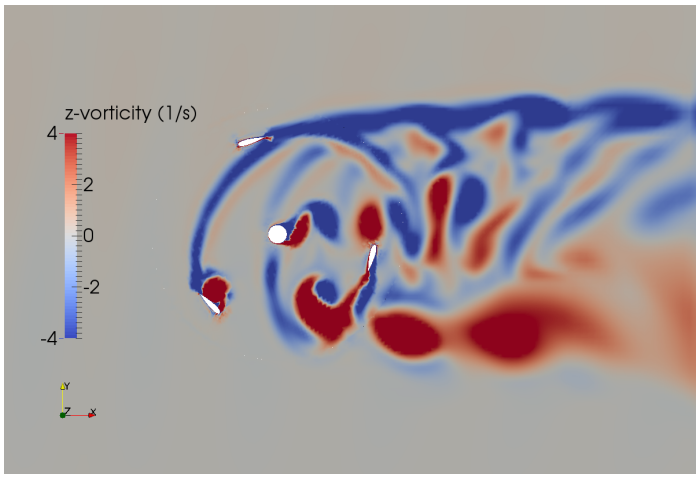

FIGURE 10. SNAPSHOT OF IN-PLANE VORTICITY CONTOURS COMPUTED BY THE 2-D RANS MODEL FOR $Re_D = 1.0 \times 10^6$. FLOW IS FROM LEFT TO RIGHT.

tank, i.e., the velocity at the walls is set fixed to the freestream value.

A sample in-plane vorticity contour plot is shown in Figure 10. Flow is from left to right. To describe the flow field at this point in the turbine rotation briefly: The blade on the lower left (1) is at high angle of attack with respect to the relative flow and has entered stall, with a large positive vortex being shed on the suction side. The blade preceding it (2) has almost reached the vortices being shed by the circular shaft, and has just moved through the major dynamic stall vortex pair created by the third blade (3, now at the top of the figure), which was created when blade (3) was in the position now occupied by blade (1). It is difficult to fully describe the very dynamic flow through a cross-flow turbine without an animation; suffice it to say that the blade-flow phenomena observed give additional insight and lend further credibility to the turbulence and Reynolds stress profiles reported in [15].

RESULTS

Performance

Mean power and drag coefficients for both the experiments and numerical simulations run at $\lambda = 1.9$ are plotted vs. Reynolds number in Figure 11. All statistics for the experiments were computed over an integer number of blade passages, and normalized with the values measured or predicted for $Re_D = 1.0 \times 10^6$. Note that the experimental values are normalize by the reference value from the experimental results, and the numerical values are normalized by the numerical results, hence the intersection at 1.0 for the reference Reynolds number. From the experimental results, it can be seen that the performance of the turbine increases asymptotically until about $Re_D = 0.8 \times 10^6$, where it then appears to become Reynolds number independent.

The 2-D simulations, due to effects of significantly increased blockage in the two-dimensional geometry and neglecting blade end effects, show higher absolute power coefficients compared to the experiments for the reference case, as expected. However, at lower Reynolds number the model predicts excessively low performance. This is likely due to difficulty in predicting separation due to dynamic stall, despite matching y^+ adjacent to the blade. The CFD results do show an increase in power coefficient with Reynolds number, but do not appear to become Reynolds number independent, though they appear to be approaching an asymptotic limit. This highlights an important limitation of the ability to extrapolate numerical results beyond the parameters for which they were validated. For instance, in this case the numerical and experimental power coefficients' non-normalized values match very well for $Re_D = 0.6 \times 10^6$. If experimental data were not available for the other Reynolds number it may be tempting to call the model "validated." However, if the numerical model was then used to predict full-scale performance, a significant overprediction would result. Note that we have not tested here for grid independence, so this may be an intervening factor, despite our matching the y^+ between the simulation cases.

The drag coefficients, not unexpectedly, seem to keep increasing slightly (by a few percent) with increasing Reynolds number, albeit less dramatically than the power coefficients.

Wake Characteristics

Mean streamwise velocity profiles obtained experimentally in the turbine horizontal center plane one turbine diameter downstream for various Reynolds numbers are compared in Figure 12, streamwise turbulence intensities are compared in Figure 13, and Reynolds stress is compared in Figure 14. The mean streamwise velocity profiles are virtually identical, showing no Reynolds

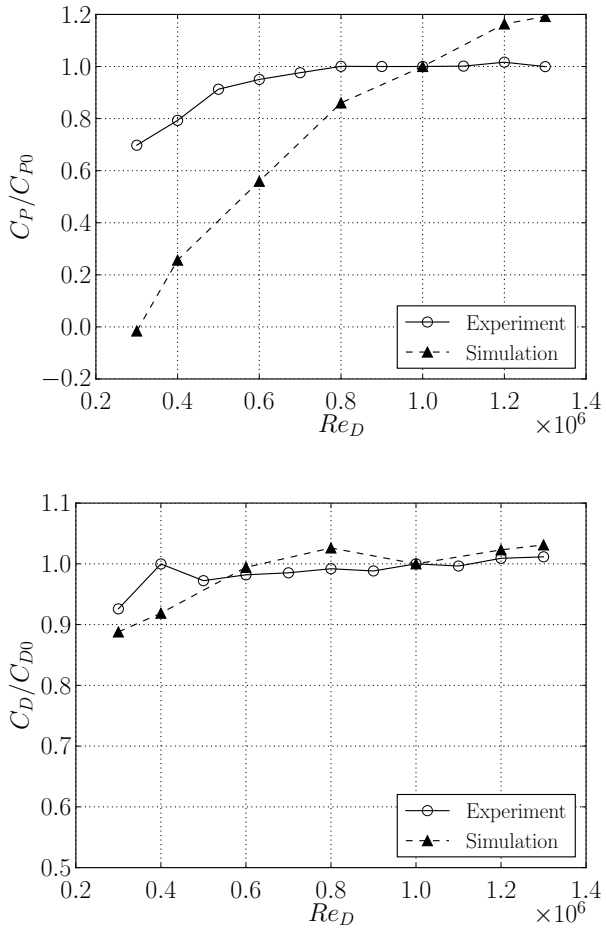

FIGURE 11. REYNOLDS NUMBER DEPENDENCE ON MEAN POWER (TOP) AND DRAG (BOTTOM) COEFFICIENTS FOR BOTH EXPERIMENTS AND COMPUTATIONS, NORMALIZED BY THE REFERENCE VALUE $C_{P0} = C_P(Re_D = 10^6)$ FOR EACH CASE.

number dependence between all cases. The turbulence intensity and Reynolds stress profiles agree well with respect to at what y/R the peaks occur, but show some difference in their magnitudes. The turbulence thus still exhibits some Reynolds number dependence for the lowest case $Re_D = 0.4 \times 10^6$.

The 2-D CFD results at four Reynolds numbers are compared to each other and an experimental reference case at $Re_D = 1.0 \times 10^6$ in Figures 15–17. Mean streamwise velocity profiles are compared in Figure 15. For the reference case, the numerical model does a reasonable job matching experiments on the left ($-y$) side of the turbine, but does poorly on the right. Significant Reynolds number dependence is also present in the CFD results, both in the shape and overall mean velocity deficit. The 2-D CFD results for mean streamwise velocity also exhibit more significant blockage than the 3-D experiments, as evidenced by

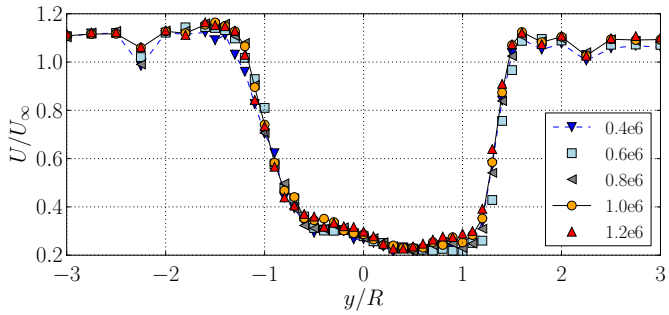

FIGURE 12. REYNOLDS NUMBER DEPENDENCE OF STREAMWISE MEAN VELOCITY; EXPERIMENTAL DATA. LEGEND ENTRIES INDICATE TURBINE DIAMETER REYNOLDS NUMBER.

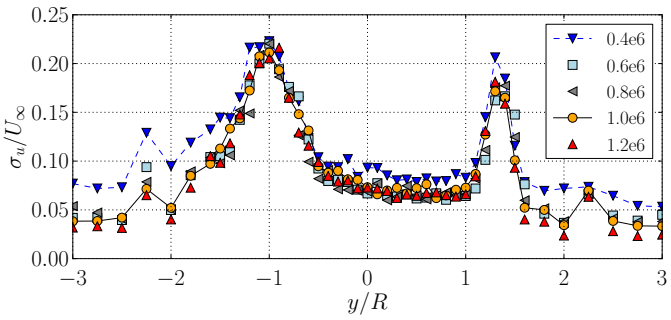

FIGURE 13. REYNOLDS NUMBER DEPENDENCE OF STREAMWISE TURBULENCE INTENSITY; EXPERIMENTAL DATA. LEGEND ENTRIES INDICATE TURBINE DIAMETER REYNOLDS NUMBER.

the higher "free stream" velocities in the "numerical tow tank" on both sides outside the turbine wake. This is physical, since blockage in 2-D is significantly higher than on 3-D. Note that a simple correction was attempted by expanding the extent of the computation domain in the y-direction, without much improvement with regards to the experimental results. This makes sense since matching blockage in 2-D increases distance to the boundary significantly.

Streamwise turbulence intensity, shown in Figure 16 matches up reasonably well between experiment and 2-D simulation for $Re_D = 1.0 \times 10^6$ on the left side of the rotor (looking upstream), whereas the peak on the right side of the rotor is not captured by the simulation. The simulations exhibit relatively large Reynolds number dependence of the turbulence quantities, with both turbulence intensity and Reynolds stress increasing with increasing Reynolds numbers, which does not agree with the trend in the experimental results. The 2-D simulations offer valuable insight into the wake dynamics of this turbine, but

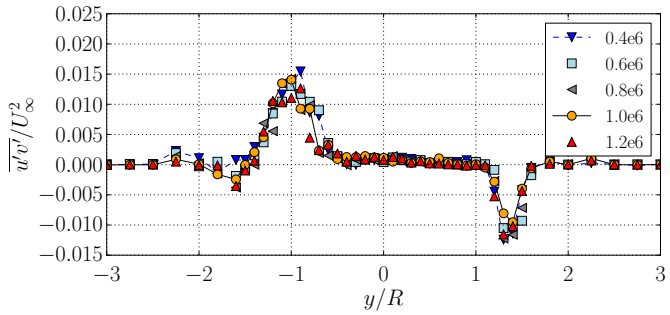

FIGURE 14. REYNOLDS NUMBER DEPENDENCE OF $\overline{u'v'}$ REYNOLDS STRESS; EXPERIMENTAL DATA. LEGEND ENTRIES INDICATE TURBINE DIAMETER REYNOLDS NUMBER.

must be viewed as preliminary until further verification, validation, and/or results from 3-D simulations are available.

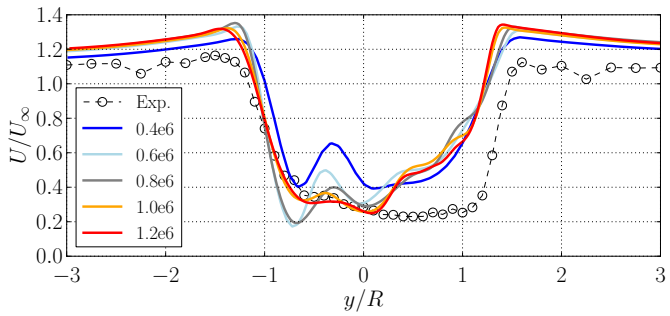

FIGURE 15. REYNOLDS NUMBER DEPENDENCE OF MEAN STREAMWISE VELOCITY; EXPERIMENT (REFERENCE CASE AT $Re_D = 1.0 \times 10^6$) VERSUS PRELIMINARY 2-D CFD RESULTS. LEGEND ENTRIES INDICATE TURBINE DIAMETER REYNOLDS NUMBER.

CONCLUSIONS

Experiments and numerical simulations were performed for a cross-flow turbine at Reynolds number based on turbine diameter from $Re_D = 0.3 \times 10^6$ to $Re_D = 1.3 \times 10^6$ to investigate Reynolds number effects on performance and near-wake characteristics.

The experimental results presented seem to indicate that the performance of the UNH-RVAT cross-flow turbine becomes Reynolds number independent at $Re_D \approx 10^6$, corresponding to an average blade chord Reynolds number $Re_c \equiv \lambda U_\infty c/\nu \approx 2 \times 10^5$. From the experimental results, no significant Reynolds number

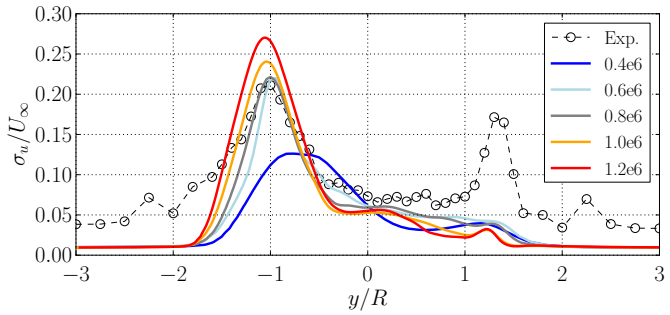

FIGURE 16. REYNOLDS NUMBER DEPENDENCE OF STREAMWISE TURBULENCE INTENSITY; EXPERIMENT (REFERENCE CASE AT $Re_D = 1.0 \times 10^6$) VERSUS PRELIMINARY 2-D CFD RESULTS. LEGEND ENTRIES INDICATE TURBINE DIAMETER REYNOLDS NUMBER.

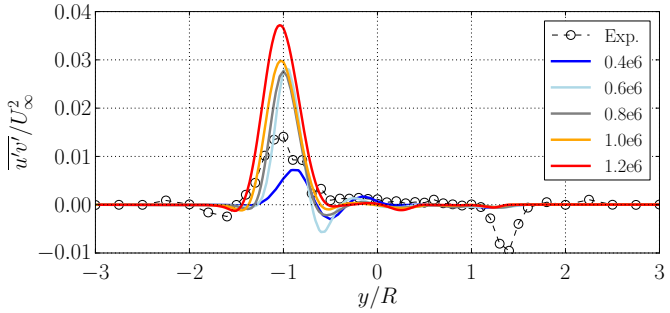

FIGURE 17. REYNOLDS NUMBER DEPENDENCE OF $\overline{u'v'}$ REYNOLDS STRESS; EXPERIMENT (REFERENCE CASE AT $Re_D = 1.0 \times 10^6$) VERSUS PRELIMINARY 2-D CFD RESULTS. LEGEND ENTRIES INDICATE TURBINE DIAMETER REYNOLDS NUMBER.

dependence was found for mean streamwise velocity profiles, however, and a very small Reynolds number dependence was observed for turbulence intensity and Reynolds stresses.

Preliminary results from 2-D RANS simulations with a k–ω SST turbulence closure model over-predict performance for the reference case of $Re_D = 1.0 \times 10^6$, due to the increased blockage in two versus three dimensions, and the exclusion of tip effects. The numerical results show much stronger Reynolds number dependence than the experimental results. Mean velocity and turbulence profiles obtained with the 2-D simulation compare reasonably well with experiments on one side of the turbine for the reference case, but show exaggerated Reynolds number dependence. This lends credibility to the numerical approach taken here, though shows that great care must be taken during verification and validation to apply the model at varying scales.

Future work will include three dimensional simulations, and analysis of Reynolds number effects on cross-stream and vertical components of the near-wake flow from both simulations and experiments. Ultimately, this research seeks to produce a more accurate parameterization—or actuator model—for improving turbine array engineering.

ACKNOWLEDGMENT

The authors would like to acknowledge funding through a National Science Foundation CAREER award (PI Wosnik, NSF-CBET 1150797, program manager Dr. Gregory Rorrer), a grant through the Leslie S. Hubbard Marine Program Endowment to purchase acoustic flow measurement instrumentation, and a grant for laboratory infrastructure upgrades through the US Department of Energy. The authors also thank Vincent Lyon for assistance during the experiments.

REFERENCES

[1] U.S. Energy Information Administration, 2012. Annual energy outlook 2012. Tech. rep., U.S. Department of Energy.

[2] Ocean Renewable Power Company, 2012. America's first ocean energy delivered to the grid, September.

[3] Alaska Energy Wiki, 2014. Hydrokinetic energy (in-river, tidal, and ocean current).

[4] Instream Energy, 2014. Project profile: Roza Canal Yakima hydrokinetic project, January.

[5] Sutherland, H. J., Berg, D. E., and Ashwill, T. D., 2012. A retrospective of VAWT technology. Tech. rep., Sandia National Laboratories.

[6] Paulsen, U. S., Pedersen, T. F., Madsen, H. A., Enevoldsen, K., Nielsen, P. H., Hattel, J., Zanne, L., Battisti, L., Brighenti, A., Lacaze, M., Lim, V., Heinen, J. W., Berthelsen, P. A., Carstensen, S., de Ridder, E.-J., van Bussel, G., and Tescione, G., 2011. "Deepwind an innovative wind turbine concept for offshore". In Proceedings of EWEA.

[7] Li, Y., and Calsal, S. M., 2010. "Modeling of twin-turbine systems with vertical axis tidal current turbines: Part Ipower output". *Ocean Engineering,* ***37***, pp. 627–637.

[8] Dabiri, J., 2011. "Potential order-of-magnitude enhancement of wind farm power density via counter-rotating vertical-axis wind turbine arrays". *Journal of Renewable and Sustainable Energy,* ***3***.

[9] Amaral, S., Perkins, N., Giza, D., and McMahon, B., 2011. Evaluation of fish injury and mortality associated with hydrokinetic turbines. Tech. Rep. 1024569, Electric Power Research Institute.

[10] Castro-Santo, T., and Haro, A., 2012. Survival and behavior of juvenile atlantic salmon and adult american shad on exposure to a hydrokinetic turbine. Tech. rep., Electric Power Research Institute.

[11] Paraschivoiu, I., 2002. *Wind Turbine Design with Emphasis on Darrieus Concept*, 1st ed. Polytechnic International, Montreal, Quebec, Canada.

[12] Sheldahl, R., and Klimas, P., 1981. Aerodynamic characteristics of seven symmetrical airfoil sections through 180-degrees angle of attack for use in aerodynamic analysis of vertical axis wind turbines. Final report SAND80-2114, Sandia National Laboratories, Albuquerque, NM, March.

[13] Yang, B., and Shu, X. W., 2012. "Hydrofoil optimization and experimental validation in helical vertical axis turbine for power generation from marine current". *Ocean Engineering,* ***42***, pp. 35–46.

[14] Bravo, R., Tullis, S., and Ziada, S., 2007. "Performance testing of a small vertical-axis wind turbine". In Proceedings of the 21st Canadian Congress of Applied Mechanics CANCAM.

[15] Bachant, P., and Wosnik, M., 2013. "Performance and near-wake measurements for a vertical axis turbine at moderate Reynolds number". In Proceedings of the ASME Fluids Engineering Division Summer Meeting, no. FEDSM2013-16575.

[16] Barone, M., Griffith, T., and Berg, J., 2011. Reference model 2: rev 0 rotor design. Tech. Rep. SAND2011-9306, Sandia National Laboratories, November.

[17] Fiedler, A. J., and Tullis, S., 2009. "Blade offset and pitch effects on a high solidity vertical axis wind turbine". *Wind Engineering,* ***33***, pp. 237–246.

[18] Neary, V., Fontaine, A., Bachant, P., Wosnik, M., Michelen, C., Meyer, R., Gunawan, B., and Straka, W., 2013. "US Department of Energy (DOE) national lab activities in marine hydrokinetics: Scaled model testing of DOE reference turbines". In Proceedings of European Wave and Tidal Energy Conference EWTEC.

[19] Menter, F., 1994. "Two-equation eddy-viscosity turbulence models for engineering applications". *AIAA Journal,* ***32***, pp. 1598–1605.